PERGAMON

International Journal of Solids and Structures 38 (2001) 423–433

INTERNATIONAL JOURNAL OF SOLIDS and STRUCTURES

www.elsevier.com/locate/ijsolstr

Biaxial bending–axial force elastic interaction diagrams in hollow steel sections

R. Irles Más *, F. Irles Más

Department of Civil Engineering, University of Alicante, Apdo. Correos 99, E-03080 Alicante, Spain

Received 24 June 1999; in revised form 16 December 1999

Abstract

Interaction diagrams are extensively used as a practical tool for designing prismatic members subjected to several combined stresses. For a long time, sets of these graphs have been available in building technologies such as reinforced concrete, steel and composite sections, under different combinations of loadings.

This paper will present the general formulation for obtaining the diagrams corresponding to biaxial bending with axial force on hollow steel sections; with circular, rectangular and square shape, with or without rounded edges. In particular, a detailed general analysis of the elastic interaction surface is made for these stresses over the above-cited sections.

Keywords: Interaction limit surface; Biaxial bending; Hollow steel section

1. Introduction

The indisputable convenience of using interaction diagrams with several combined loadings (generally up to 3), on a prismatic member section, is the cause for the spread of these graphs. It should be mentioned that, among them, those corresponding to reinforced concrete sections are elaborated by Jiménez Montoya et al. (1991), as being universal. It could also be cited that those are available for metallic or mixed profiles in several publications, among which stand out the works by Atsuta and Chen (1976), Zhou and Chen (1985) and Bradford (1991).

This paper presents the general approach that allows the analytical formulation of biaxial bending–axial force interaction diagrams in the usual hollow metallic sections, for the situation in which the most stressed point yields. We study the general case of rectangular sections with rounded edges, which allows one to extend conclusions to cases of sharp edges, at one end, and to that of a circular section, at the other, as they are both particular conditions of the general case.

* Corresponding author. Fax: +34-9-6590-3678.
E-mail address: dicop@ua.es (R. Irles Más).

0020-7683/00/$ - see front matter
PII: S0020-7683(00)00045-7

2. General approach to the problem

For a hollow rectangular metallic section with rounded edges (Fig. 1), subjected to tension or compression force and biaxial bending, the most stressed point is one in the outer contour on one of the corners. All the points on one side of the outer contour share the maximum value when bending is uniaxial.

Given the double symmetry of these sections, it suffices to study the quadrant showing greater stresses, which will be the one furthest away from the neutral fiber. Therefore, with the notation of that figure, we have

The general expression for the tensions:

$$\sigma(x,y) = \frac{N}{A} + \frac{M_x}{I_x}y + \frac{M_y}{I_y}x \tag{1}$$

that will be written as follows:

$$\sigma(x,y) = v + \mu_x y + \mu_y x. \tag{2}$$

The equation for neutral fiber is

$$o = v + \mu_x y + \mu_y x;\ y_{\mathrm{NF}} = -\frac{\mu_y}{\mu_x}x - \frac{v}{\mu_x}. \tag{3}$$

Following the usual criterion in metallic structures of taking, as the maximum demand, the combination of loading that reaches the yield stress σ_e at the most stressed point, the limit condition will be

$$\sigma_e = v + \mu_x y_{\max} + \mu_y x_{\max}. \tag{4}$$

Since stresses (1) are linear, the maximum stress point $(x_{\max}, y_{\max})$ will be the one furthest away from the neutral fiber, inside that circular contour, i.e., that in which the tangent to the circle is parallel to the neutral fiber.

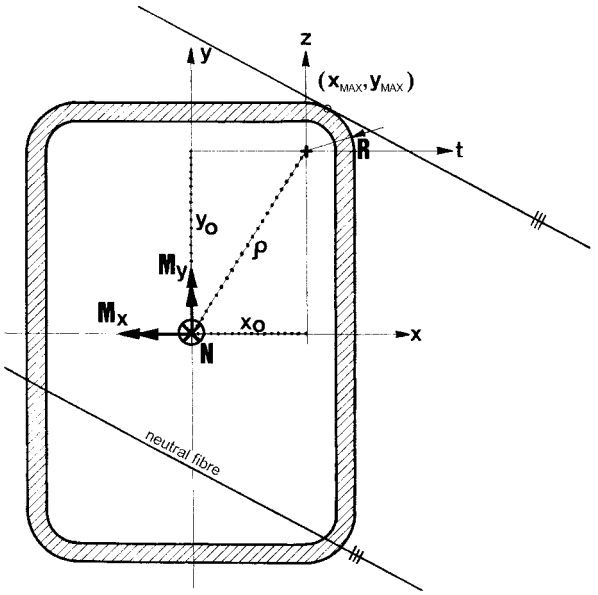

Fig. 1. Geometrics and stresses of a hollow section.

Circumference

$$z = \sqrt{R^2 - t^2}. \tag{5}$$

Parallelism requires

$$z' = \frac{\mathrm{d}z}{\mathrm{d}t} = \left(\frac{\mathrm{d}y}{\mathrm{d}x}\right)_{\mathrm{NF}} \Rightarrow \frac{t_{\max}}{\sqrt{R^2 - t_{\max}^2}} = \frac{\mu_y}{\mu_x}$$

that is

$$t_{\max} = \frac{R\mu_y}{\sqrt{\mu_x^2 + \mu_y^2}},$$

and from Eq. (5)

$$z_{\max} = \frac{R\mu_x}{\sqrt{\mu_x^2 + \mu_y^2}}.$$

In the main central axes

$$x_{\max} = x_0 + \frac{R\mu_y}{\sqrt{\mu_x^2 + \mu_y^2}},$$

$$y_{\max} = y_0 + \frac{R\mu_x}{\sqrt{\mu_x^2 + \mu_y^2}}.$$

Therefore, the limit condition (4) will be

$$\sigma_{\mathrm{e}} = v + \mu_x\left(y_0 + \frac{R\mu_x}{\sqrt{\mu_x^2 + \mu_y^2}}\right) + \mu_y\left(x_0 + \frac{R\mu_y}{\sqrt{\mu_x^2 + \mu_y^2}}\right). \tag{6}$$

After rationalizing, squaring and placing everything in order, the results are as follows:

$$v^2 + (y_0^2 - R^2)\mu_x^2 + (x_0^2 - R^2)\mu_y^2 + 2y_0 v\mu_x + 2x_0 v\mu_y + 2x_0 y_0 \mu_x\mu_y - 2\sigma_{\mathrm{e}} v - 2\sigma_{\mathrm{e}} y_0\mu_x - 2\sigma_{\mathrm{e}} x_0\mu_y + \sigma_{\mathrm{e}}^2 = 0, \tag{7}$$

equation for the limit surface, which turns out to be a quadric in the axes (v, μ_x, μ_y) as well as in axes N, M_x, M_y.

3. Study of the limit surface

3.1. General case

Expression (7) represents a quadric surface with axes oblique to axes (v, μ_x, μ_y). The study and classification of this surface could easily be made consulting any algebra textbook (García and López, 1984).

Since the determinant

$$\begin{vmatrix} 1 & y_0 & x_0 & -\sigma_e \\ y_0 & y_0^2 - R^2 & x_0 y_0 & -\sigma_e y_0 \\ x_0 & x_0 y_0 & x_0^2 - R^2 & -\sigma_e x_0 \\ -\sigma_e & -\sigma_e y_0 & -\sigma_e x_0 & \sigma_e^2 \end{vmatrix} = 0 \quad \forall \sigma_e, x_0, y_0, R.$$

Eq. (7) represents a cone for all cases.

Its center (v_c, v_{xc}, v_{yc}) is the solution of

$$\begin{vmatrix} 1 & y_0 & x_0 \\ y_0 & y_0^2 - R^2 & x_0 y_0 \\ x_0 & x_0 y_0 & x_0^2 - R^2 \end{vmatrix} \begin{vmatrix} v_c \\ \mu_{xc} \\ \mu_{yc} \end{vmatrix} = \begin{vmatrix} \sigma_e \\ \sigma_e y_0 \\ \sigma_e x_0 \end{vmatrix} \Rightarrow \begin{vmatrix} v_c = \sigma_e \Rightarrow N = A\sigma_e, \\ \mu_{xc} = 0, \\ \mu_{yc} = 0 \end{vmatrix}$$

that is, in all cases, it is located at N axis, at $N_u = A\sigma_e$.

Its main axes are the eigenvectors corresponding to the eigenvalues for this coefficient matrix:

$$\begin{vmatrix} 1-\lambda & y_0 & x_0 \\ y_0 & y_0^2 - R^2 - \lambda & x_0 y_0 \\ x_0 & x_0 y_0 & x_0^2 - R^2 - \lambda \end{vmatrix} = 0 = \lambda^3 + \lambda^2(2R^2 - 1 - \rho^2) + \lambda(R^4 - R^2\rho^2 - 2R^2) - R^4,$$

where $\rho^2 = x_0^2 + y_0^2$ (Fig. 1).

The solutions to this equation are

$$\lambda_1 = \frac{1 + \rho^2 - R^2 + \sqrt{(R^2 - 1 - \rho^2)^2 + 4R^2}}{2} > 0,$$

$$\lambda_2 = \frac{1 + \rho^2 - R^2 - \sqrt{(R^2 - 1 - \rho^2)^2 + 4R^2}}{2} < 0,$$

$$\lambda_3 = -R^2 < 0,$$

and the corresponding eigenvectors (not normalized) are

$$\vec{v}_1 = \left(\frac{1 + R^2 - \rho^2 + \sqrt{(R^2 - 1 - \rho^2)^2 + 4R^2}}{2}, y_0, x_0 \right),$$

$$\vec{v}_2 = \left(\frac{1 + \rho^2 - R^2 - \sqrt{(R^2 - 1 - \rho^2)^2 + 4R^2}}{2}, y_0, x_0 \right),$$

$$\vec{v}_3 = (0, -x_0, y_0).$$

A group of axes $(m, n, \tilde{n})$ parallel to these vectors in the center of the cone $(A\sigma_e, 0, 0)$ will become the main axes for the quadric. The one parallel to $\vec{v}_1$ is the cone axis, since $\lambda_1 > 0$. Carrying out a change of axes to the main ones (m being the cone axis), the equation for the quadric is reduced to

$$\lambda_1 m^2 + \lambda_2 n^2 + \lambda_3 \tilde{n}^2 = 0,$$

which allows us to identify it, in general ($\lambda_2 \neq \lambda_3$) as a cone with an elliptical directrix and an m axis oblique to the coordinate planes for the case of rectangular hollow sections with rounded vertices.

3.2. Particular cases

3.2.1. Rectangular section without rounded corners

In this case, with $R = 0$ and $(x_{\max}, y_{\max}) = (x_0, y_0)$, the results obtained are

$$\lambda_1 = 1 + \rho^2, \quad \lambda_2 = \lambda_3 = 0.$$

The cone semiangle values are $\pi/2$ and it degenerates into a double plane, with an immediate equation from expression (1):

$$\sigma_e = \frac{N}{A} + \frac{M_x}{I_x} y_0 + \frac{M_y}{I_y} x_0,$$

which goes through all three points $N_u = A\sigma_e$, $M_{xu} = \sigma_e I_x / y_0$, $M_{yu} = \sigma_e I_y / x_0$ (Fig. 2).

3.2.2. Square section without rounded corners

In this case, the tracing of the plane constituting the interaction surface with that for $N = 0$ is parallel to its second bisectrix.

3.2.3. Circular section

In this case, $x_0 = y_0 = 0 = \rho$ and R is the section's outer radius. The results are

$$\lambda_1 = 1, \quad \lambda_2 = -R^2, \quad \lambda_3 = -R^2$$

and the cone turns out to have a circular directrix. Its axis, oblique, in the general case, to coordinate planes, now coincides with the axis for axial force (Fig. 3), since the first eigenvector is, now normalized: $\vec{v}_1 = (1, 0, 0)$.

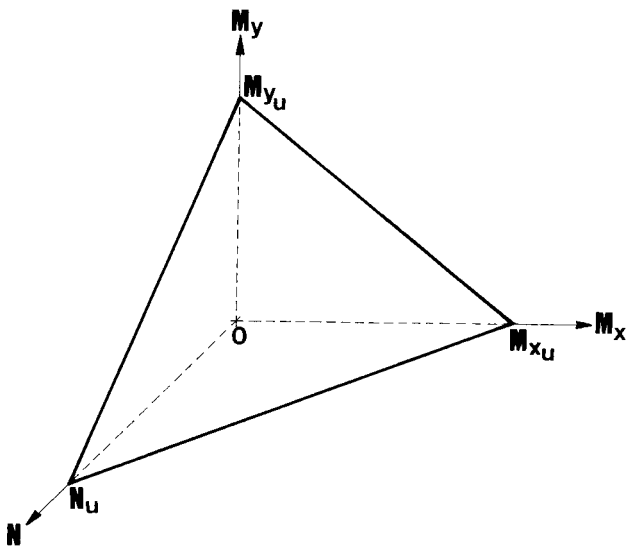

Fig. 2. Interaction surface for a sharp corner rectangular section.

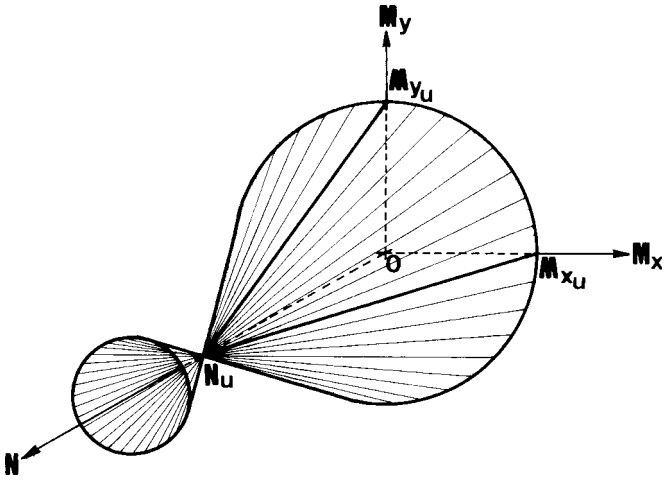

Fig. 3. Interaction surface for a circular section.

4. Representation of the limit surface: interaction diagrams

4.1. Circular section

Fig. 4 represents the portion of interaction surface contained in the first octant, which is the only one to be considered taking into account how the problem has been set up. In the figure, the bidimensional reality of the problem could be appreciated. The surface representation can be reduced to a straight line in the NOM_r plane, $M_r = \sqrt{M_x^2 + M_y^2}$ being the resulting bending. The N–M_r interaction diagram for the corresponding circular section is comprised of a single straight line in this case. Fig. 5 represents the interaction diagram corresponding to a profile with diameter 100 mm and thickness 5 mm ($\sigma_e = 254.8 \times 10^6$ Pa).

Contour lines $N =$ constant of the surface are concentric circumferences with the origin, and constitute the interaction diagram in a group of arbitrary axes which do not coincide with that of the resulting bending.

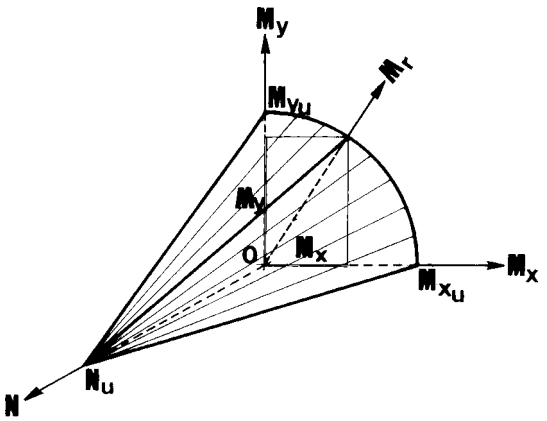

Fig. 4. Reduction of surface to a single straight line.

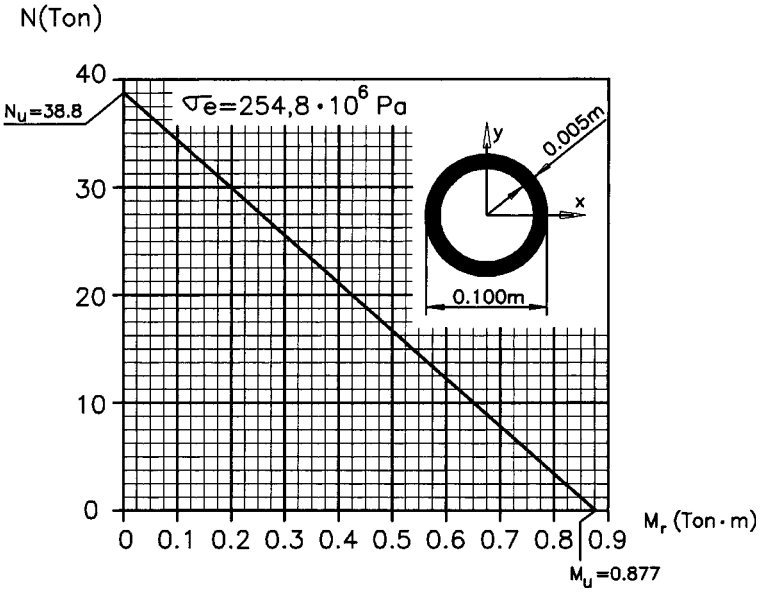

Fig. 5. Interaction diagram for a circular section.

4.2. Rectangular section with sharp corners

Fig. 6 represents the portion in the first octant of the plane where the general case degenerates. In this case, the problem is tridimensional, and all flat sections are parallel straight lines for constant values for any of the three variables. Representing, for instance, contour lines $N=$ constant of the interaction surface, an interaction diagram is obtained, like that in Fig. 7, which constitutes one of the possible N–M_x–M_y interaction diagrams for this type of section.

When the section is square, and in the option mentioned of cutting with $N=$ constant planes, the straight lines in the interaction diagram are parallel to the second bisectrix for the M_x–M_y plane, given the double symmetry of the section.

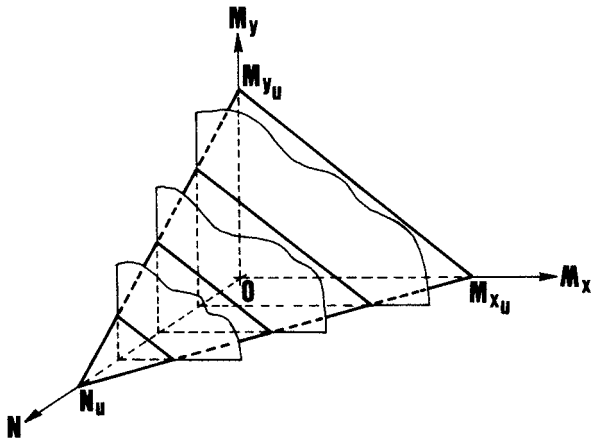

Fig. 6. Generation of graphs for a sharp-edged rectangular sections.

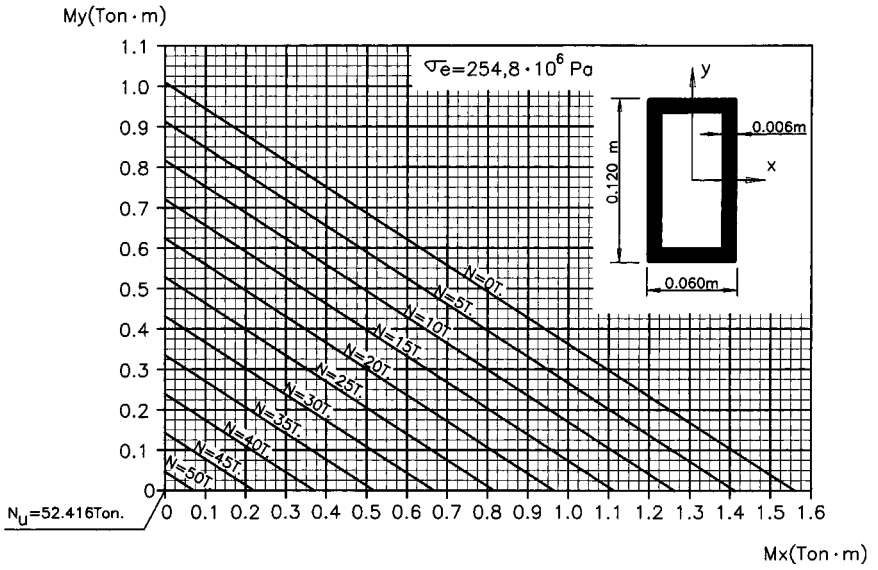

Fig. 7. Interaction diagram for a sharp-edged rectangular section.

Fig. 7 shows the diagram corresponding to a rectangular profile of 120×60 mm^2 and 6 mm of thickness with sharp corners ($\sigma_e = 254.8\times10^6$ Pa).

4.3. Rectangular section with rounded corners

Bearing in mind the shape of the interaction surface in the general case, the intersections with the planes parallel to the coordinate ones are all conical curves, except those corresponding to the NOM_x and NOM_y planes. These are straight lines, since the ON axis goes through the center of the cone, now with an axis oblique to those planes.

If, as before, the interaction surface is represented by means of its contour lines, $v = k$ (which constitutes one of the possible options, probably the most usual and convenient one), these result in the following equation, from Eq. (7):

$$\mu_x^2(y_0^2 - R^2) + \mu_y^2(x_0^2 - R^2) + 2(k - \sigma_e)y_0\mu_x + 2(k - \sigma_e)x_0\mu_y + 2x_0y_0\mu_x\mu_y + (k - \sigma_e)^2 = 0,$$

which always represents conical lines. To study its classification, the main axes are obtained next:

$$\begin{vmatrix} y_0^2 - R^2 - \lambda & x_0y_0 \\ x_0y_0 & x_0^2 - R^2 - \lambda \end{vmatrix} = 0 = \lambda^2 + \lambda(2R^2 - \rho^2) + R^2(R^2 - \rho^2).$$

Eigenvalues

$$\lambda_{\mathrm{I}} = \rho^2 - R^2 > 0, \qquad \lambda_{\mathrm{II}} = -R^2 < 0.$$

Unitary eigenvectors

$$\vec{v}_{\mathrm{I}} = \left(\frac{y_0}{\rho}, \frac{x_0}{\rho}\right), \qquad \vec{v}_{\mathrm{II}} = \left(-\frac{x_0}{\rho}, \frac{y_0}{\rho}\right)$$

carrying out the change to the (ξ, η) axes, given by $\vec{v}_{\mathrm{I}}, \vec{v}_{\mathrm{II}}$, results, in a canonical way, in

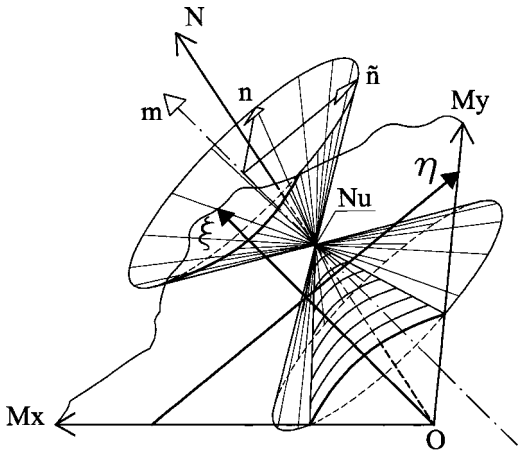

Fig. 8. The oblique cone in the general case.

$$\frac{\left[\xi+\frac{(k-\sigma_e)\rho}{\rho^2-R^2}\right]^2}{\left[\frac{(k-\sigma_e)R}{\rho^2-R^2}\right]^2}-\frac{\eta^2}{\left[\frac{k-\sigma_e}{\sqrt{\rho^2-R^2}}\right]^2}=1$$

that is to say, non-equilateral hyperbolas with a center $[\rho(\sigma_e-k)/(\rho^2-R^2),0]$ in the axes (ξ,η). The one corresponding to $N=0$ is shown in Fig. 8 on the M_x–M_y plane. The branch which is nearest to the origin, corresponding to the cone leaf developed on its semiaxis not included in the first octant, cuts the axes OM_x and OM_y, at the points

$$M_{xu}=\frac{I_x\sigma_e}{y_0+R},\qquad M_{yu}=\frac{I_y\sigma_e}{x_0+R}.$$

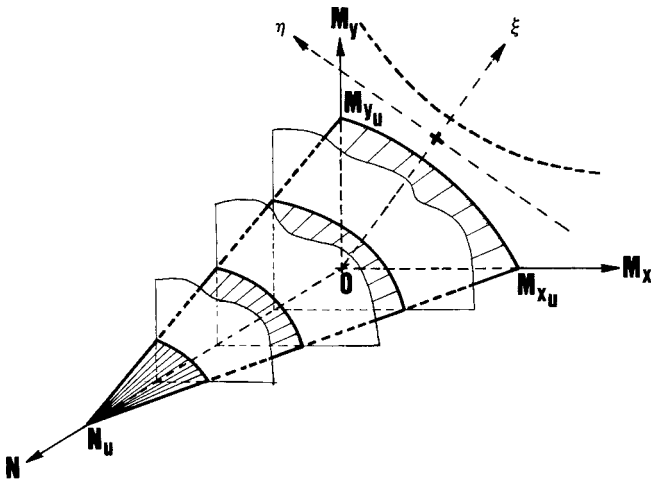

Fig. 9. Generation of diagrams in the general case.

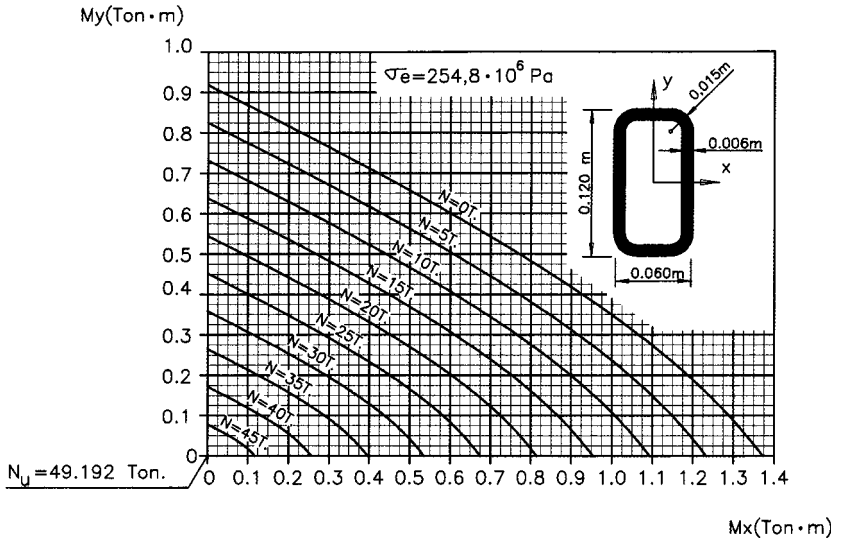

Fig. 10. Interaction diagram for a round-edged rectangular section.

The portion of this branch located between those points is the only one to be considered in the problem, since the other branch, corresponding to another cone leaf, provides values outside the problem's range.

The generation of the contour lines $v = k$ is shown in Fig. 9. Fig. 10 shows the diagram thus generated for the same 120×60 mm^2 profile, now with rounded corners, already on the N–M_x–M_y axes, ready to be used.

In the case of square profiles with rounded corners, all these considerations continue to be valid and, furthermore, the main axis ξ of the hyperbola coincides with the bisectrix of the M_x–M_y first quadrant, given the double symmetry of the section.

It is evident that the values of N, M_x, M_y represented in the diagrams must already include the corresponding ponderation coefficients, as well as that of buckling if N is a compression action.

5. Conclusion

This paper focuses on the generic shape of the biaxial bending–axial force interaction surface of hollow metallic profiles.

The approach to the problem allows the study of circular and rectangular shapes, with or without rounded corners, with a remarkable unity, as well as the specific formulation of the N–M_x–M_y interaction diagrams, for the different types of profiles.

It is shown that the interaction surface in those axes is always a cone.

In rectangular profiles with rounded corners, the cone has an elliptical directrix with its axis oblique to the coordinate planes, and its $N =$ constant contour lines result in non-equilateral hyperbolas.

In rectangular profiles with sharp corners, the cone degenerates into a double plane, and parallel straight lines define the interaction diagrams.

Finally, in circular sections, the cone has a circular directrix, its axis being the axial force one, and the diagrams traced by means of $N =$ constant are concentric circumferences. The bidimensional reality of the problem becomes evident as the resulting bending direction being indifferent. Therefore, the interaction diagram can be reduced to a single straight line in the total axial force–bending plane.

References

Atsuta, T., Chen, W.F., 1976. Theory of Beam–Columns, vol. 2. McGraw-Hill, New York.
Bradford, M.A., 1991. Design of short concrete-filled RHS sections. J. Inst. Engng. Aust.: Div. Engng. CE 33.3, 189–194.
García, J., López, M., 1984. Algebra Lineal y Geometría. Marfil, Alcoy, Spain.
Montoya, P.J., et al., 1991. Hormigón Armado, 13th edn., vol. 2. Gustavo Gili, Barcelona.
Zhou, S.P., Chen, W.F., 1985. Design criteria for box columns under biaxial loading. J. Struct. Engng. 111.12, 2643–2658.